# Synthesis and structure-activity relationship studies of original cyclic diadenosine derivatives as nanomolar inhibitors of NAD kinase from pathogenic bacteria

David A Clément, Muriel Gelin, Clarisse Leseigneur, Valérie Huteau, Lou Mondange, Jean-Luc Pons, Olivier Dussurget, Corinne Lionne, Gilles Labesse, Sylvie Pochet

# Synthesis and structure-activity relationship studies of original cyclic diadenosine derivatives as nanomolar inhibitors of NAD kinase from pathogenic bacteria

David A. Clément,[1] Muriel Gelin,[2] Clarisse Leseigneur,[3] Valérie Huteau,[1‡] Lou Mondange,[3] Jean-Luc Pons,[2] Olivier Dussurget,[3] Corinne Lionne,[2] Gilles Labesse,[2*] Sylvie Pochet[‡1*]

[1] Institut Pasteur, Université Paris Cité, CNRS UMR3523, Unité de Chimie et Biocatalyse, F-75015 Paris, France.

[2] Centre de Biologie Structurale (CBS), CNRS UMR5048, INSERM U1054, Université de Montpellier, 34090 Montpellier, France.

[3] Institut Pasteur, Université Paris Cité, CNRS UMR6047, Unité de Recherche *Yersinia*, F-75015 Paris, France.

* Corresponding author: sylvie.pochet@pasteur.fr; gilles.labesse@cbs.fr

‡ Present address: Institut Pasteur, Université Paris Cité, CNRS UMR3523, Unité de Chimie Biologique Epigénétique, F-75015 Paris, France.

## Abstract

Nicotinamide adenine dinucleotide kinases (NAD kinases) are essential and ubiquitous enzymes involved in the production of NADP(H) which is an essential cofactor in many metabolic pathways. Targeting NAD kinase (NADK), a rate limiting enzyme of NADP biosynthesis pathway, represents a new promising approach to treat bacterial infections. Previously, we have produced the first NADK inhibitor active against staphylococcal infection. From this linear di-adenosine derivative, namely NKI1, we designed macrocyclic analogues. Here, we describe the synthesis and evaluation of an original series of cyclic diadenosine derivatives as NADK inhibitors of two pathogenic bacteria, *Listeria monocytogenes* and *Staphylococcus aureus*. The nature and length of the link between the two adenosine units were examined leading to sub-micromolar inhibitors of NADK1 from *L. monocytogenes*, including its most potent *in vitro* inhibitor reported so far (with a 300-fold improvement compared to NKI1).

## Keywords

Inhibitor; macrocyclic compound; NAD kinase; crystal structure; *Staphylococcus*; *Listeria*

## 1. Introduction

Antibacterial multidrug resistance is a major public health problem requiring urgent development of new antibiotics and identification of original bacterial targets, as pointed out by the World Health Organization [1]. We have initiated a decade ago the characterization of such a new target involved in NAD biosynthesis: the nicotinamide adenine dinucleotide kinase. NAD kinases (NADK, EC 2.7.1.23) catalyse the phosphorylation of NAD to NADP, which is subsequently reduced to NADPH [2,3]. As the sole known enzyme producing NADP *de novo*, NADK plays a crucial role in controlling the intracellular balance of NAD(H) and NADP(H) in many metabolic pathways [4-6]. NADK enzymatic properties have been known for decades [7], but the genes encoding the NADK were identified more recently, leading to the discovery of orthologs in nearly all living organisms [6,8,9]. The NADKs belong to a superfamily of kinases, including 6-phosphofructokinases (PFKs), soluble diacylglyceride kinases, and sphingosine kinases [10]. In line with a low overall sequence similarity (~20% sequence identity), the human cytoplasmic and mitochondrial enzymes exhibit substantial differences compared to their bacterial counterparts [6,8,9]. Because of the essential role of NADK in all bacteria tested so far, such as *Bacillus subtilis* [11], *Mycobacterium tuberculosis* [12,13] and *Staphylococcus aureus* [14,15], NADK is considered as an attractive target for the development of novel antibiotics with an original mode of action [5,16-18].

During the last decade, we have developed a series of adenosine derivatives as potent inhibitors of recombinant *Listeria monocytogenes* and *S. aureus* NADKs [15,19-21]. The most potent molecules were found to bind to the NAD-binding site of NADK in a restricted conformation as compared to NAD thanks to the propargyl linker. One of these compounds became the first NADK inhibitor (NKI1, Figure 1) active in mice infected with *S. aureus*, including antibiotic-resistant strains [15].

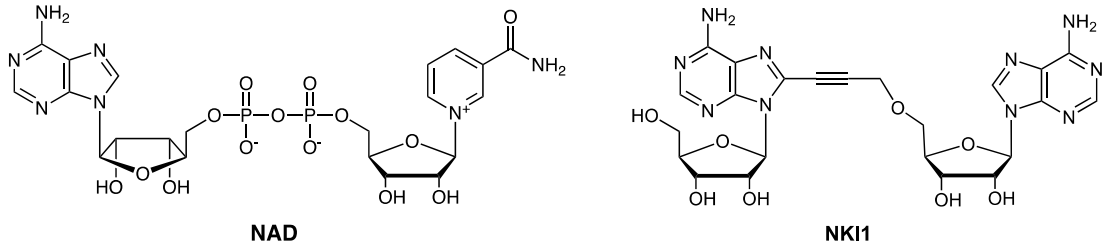


**Figure 1**: Chemical structures of NAD and NKI1

We next described the synthesis of a series of functionalized NKI1 derivatives as chemical tools to gain detailed knowledge about the mechanism of action of this lead compound [22]. Two of these new compounds harbor some chemical substitutions suggesting that macrocyclization could be envisioned to strengthen further their affinity and specificity for NADKs. The peculiar binding mode of NAD and its

analogues into the active site of NADKs suggested that a more constrained compound would gain both affinity for those NADKs and specificity over a wide range of NAD(P) binding proteins [23,24]. Indeed, macrocyclization has been demonstrated to provide ligands with higher affinity due to entropy gain upon binding [25-27]. This was successfully implemented for several therapeutic targets [28-31], but not yet applied to NADKs.

Recent progress have been made to develop cyclization strategies for macrocyclization of peptides [26], nucleosides [32] and oligonucleotides [33] or to generate libraries of macrocyclic compounds [34]. However, the synthesis of macrocycles is generally challenging since the ring-closing reaction efficiency depends on the size and geometry of the bridging linker. Thus, cyclization reactions do not favor the formation of large rings. Moreover, inter- instead of intra-molecular reaction is a major issue, in particular for the head-to-tail cyclization of peptides [30]. Therefore, most cyclizations need to be conducted in dilute solutions to favor macrocyclization over side product formation (dimerization or oligomerization). The ring-closing step can be achieved by a variety of chemical reactions, including amide coupling, ring-closing metathesis, nucleophilic substitution, palladium-catalyzed cross coupling reaction. The careful choice of ring disconnection and appropriate precursors can improve yields and reduce side reactions [27,29].

In the present study, we describe the synthesis of six original macrocycles (**MC1-MC6**, Figure 2) inspired by linear derivatives of compound NKI1 [15,22]. These cyclic molecules differ in the functional group introduced at the 5' position of one adenosine moiety (sulfonamide, amide, urea) and in the length of the small linking alkyl chain (5 to 8 atoms long).

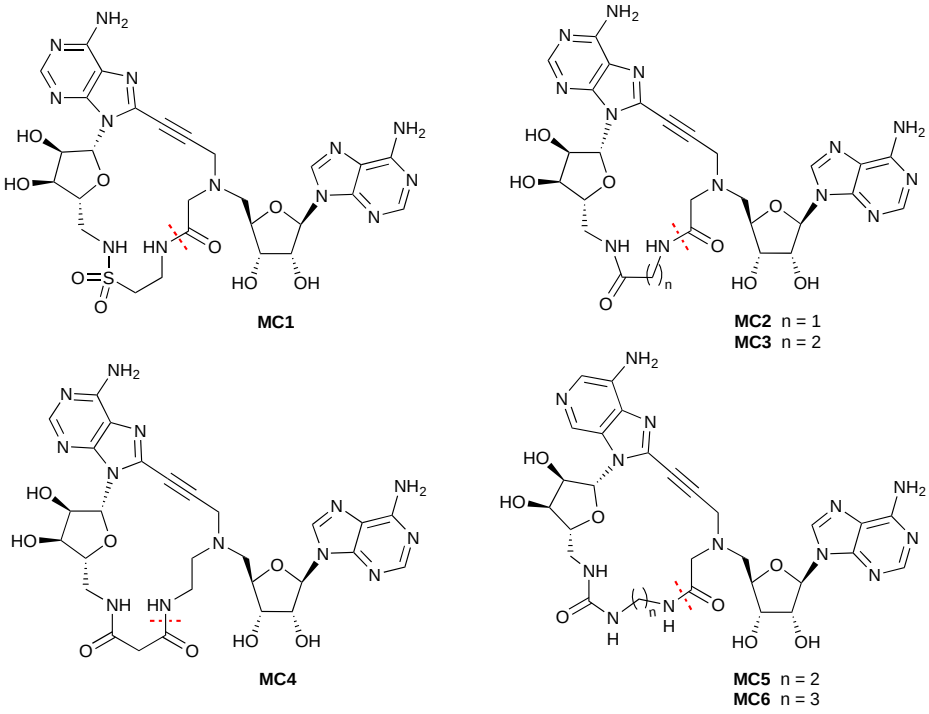


**Figure 2:** Chemical structures of macrocycles **MC1-6** (amide disconnection in red dotted lines)

The precise binding mode of the macrocycles **MC1-6** into *L. monocytogenes* NADK (*Lm*NADK1) was verified by X-ray crystallography. Their inhibitory potencies were measured *in vitro* on purified enzymes and evaluated on bacterial growth of two human pathogenic bacteria, *L. monocytogenes* and *S. aureus*. The structure-activity relationship study of this new class of inhibitors is presented hereafter.

## 2. Results and Discussion

### 2.1. Crystal structure of *Lm*NADK1 in complex with a new linear diadenosine compound

As an amide moiety at 5'-end of NKI1 has been recently shown to fit quite well into the active site of *Lm*NADK1 (PDB ID 6Z65) [22], we wondered if a sulfonamide group could accommodate as well. Such a NKI1 derivative (hereafter compound **1**, Figure 3A) was synthesized and successfully observed bound to *Lm*NADK1 by X-ray crystallography. The structural analysis of *Lm*NADK1 in complex with **1** highlighted key interactions and a special orientation of its amino-alkyl side chain in the NAD binding site of *Lm*NADK1.

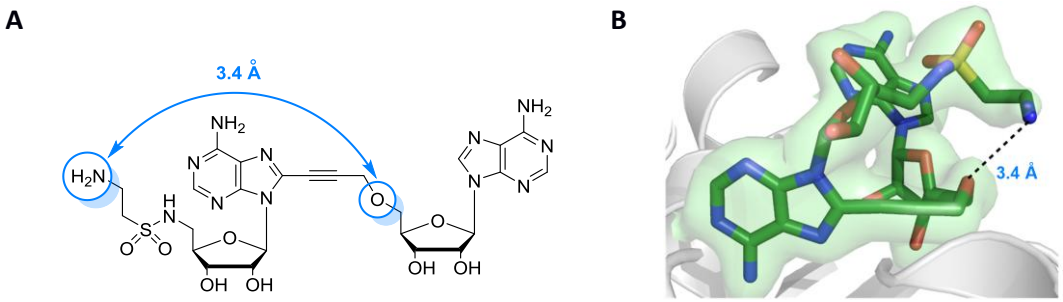


**Figure 3:** (A) Chemical structure of compound **1**. (B) X-ray crystal structure of compound **1** bound to *Lm*NADK1 (PDB ID 8A9V). Compound **1** is shown in sticks color according to cpk code with carbon in green. The electron density is shown as a green surface around the ligand. A black dashed line indicates an intramolecular hydrogen bond. The figure B was drawn using Pymol (www.pymol.org).

In particular, the X-ray structure reveals a distance of 3.4 Å between the amino group at the 5' end and the oxygen atom of the propargyl linker of compound **1** (Figure 3B). We hypothesized that joining these two positions (by an appropriate linker) would restrict the conformational flexibility of the molecule and provide more intra- and inter-molecular interactions. These properties were expected to provide more potent NADK inhibitors than **1** or its parent compound NKI1.

### 2.2. Structure-based design of novel cyclic diadenosines

From the crystal structures of *Lm*NADK1 with various nucleosidic compounds and especially the lead compound **NKI1**, we deduced possible substitutions at the 5' end of the free ribose (i.e., not yet linked to the propargyl moiety). The best possible cyclization paths from that 5' position to the polar head of the propargyl were first deduced from the position occupied by substitutions of the same ribose in various

mono-adenosines previously screened by X-ray crystallography [15,20,22]. Beside the sulfonamide group as in compound **1** (PDB ID 8A9V), an amide group will also fit well according to a recent complex (PDB ID 6Z65) [22]. From these two structures, a urea group was also envisioned to bring a stabilizing internal hydrogen bond. On the propargyl side, the main constraints learned from previous structures come from the knowledge of the orientation of the methyl group on an amino propargyl linker [15] and that of a small linear alkyl chain (PDB ID 6Z64) [22]. The resulting molecules were built virtually and docked into the binding site of *Lm*NADK1. The conformational constraints on the macrocycles were carefully evaluated after energy minimization or docking. For the most relaxed conformations, the interactions with the protein were checked. Chemical feasibility was then considered to focus on the most readily accessible compounds (illustrated in Figure 2).

**2.3. Chemistry**

The general synthetic route to macrocycles **MC1-6** is based on intramolecular cyclization of unprotected linear (acyclic) precursors through an amide bond formation. Amide formation was selected for the final ring-closure reaction, as it is compatible with the functionalities of nucleosidic components. The necessary carboxylic acid and amine functional groups were introduced at a determined position of the linking alkyl chain (retrosynthetic disconnection, red dotted lines on Figure 2) to reduce the number of building blocks to be prepared while expecting reasonable cyclization yields. Functionalized linear precursors were obtained *via* a Sonogashira coupling reaction between two adenosine derivatives bearing either a terminal alkyne or a bromide (as depicted in Scheme 1).

*Synthesis of the target compound **MC1***

The synthesis of **MC1** is depicted in Scheme 1. The key intermediate **2b** was obtained in two steps from 2',3'-*O*-protected adenosine via Staudinger reduction of the 5'-azido-derivative **2a** [21,22]. Further reaction of **2b** with commercially available 2-phtalimidoethanesulfonyl chloride, followed by hydrazinolysis of phthalimide **3a**, *N*-Boc protection and C-8 bromination, resulted in the formation of bromide **4**. On the other hand, alkyne **6** was obtained starting from **2b** by selective 5'-*N*-propargylation *via* the nosyl strategy [35], followed by reaction of **5** with ethyl bromoacetate. Sonogashira reaction of **4** with **6** gave the coupling product **7** in moderate yield. Two-step global deprotection resulted in the diadenosine **8** as TFA salt. Attempts to further purify the crude product by reverse phase HPLC using 10 mM TEAA buffer (pH 6) resulted in the formation of unknown compounds. Intramolecular cyclization into **MC1** was achieved by reaction of crude **8** with PyBOP in the presence of DIEA in DMF under high-dilute condition.

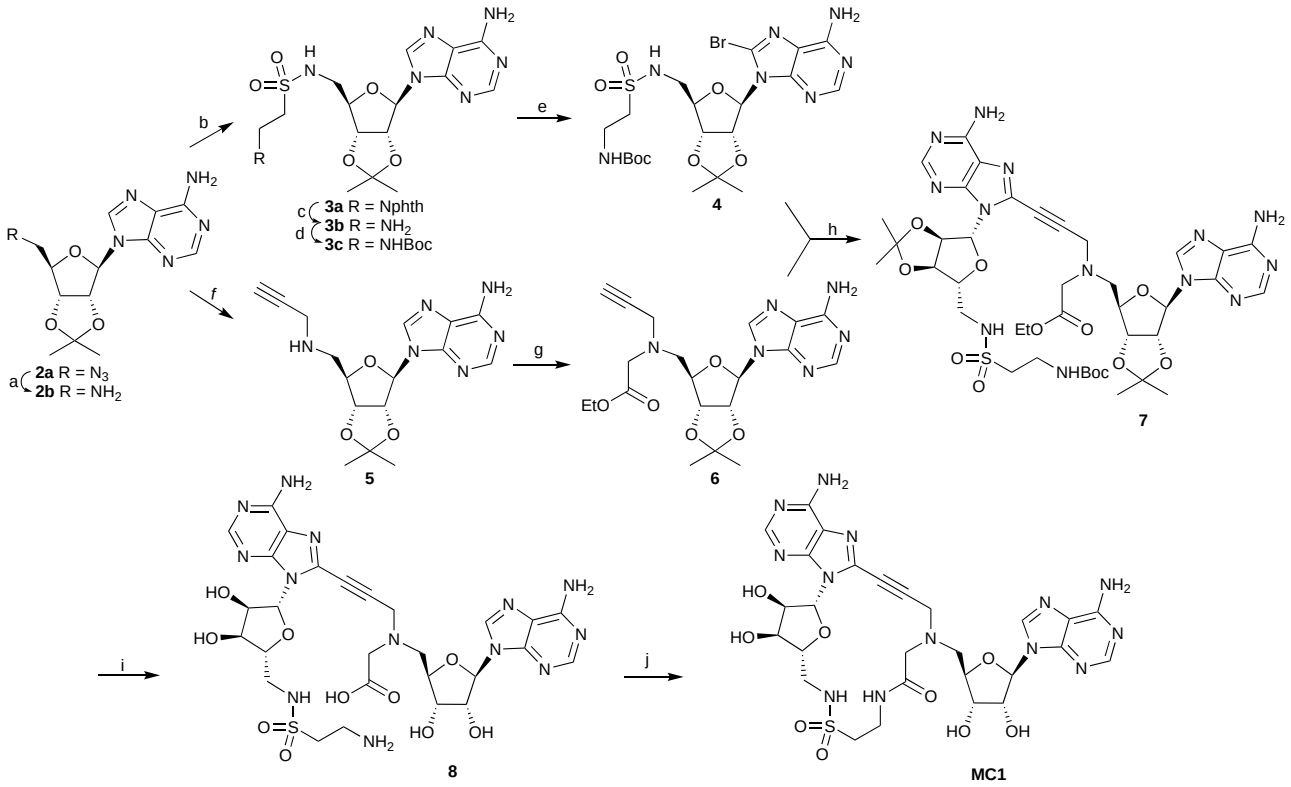


**Scheme 1:** Synthesis of **MC1**

*Reagents and conditions:* (a) $PPh_3$, pyridine, 3 h, then $NH_4OH$, 4h, 92%; (b) $PhthNCH_2CH_2SO_2Cl$, TEA, DMF, rt, 1 h; (c) Hydrazine hydrate, EtOH, rt, 5 h, 49% from **2b**; (d) $Boc_2O$, DMF, rt, 18 h, 84%; (e) $Br_2$, dioxane/acetate buffer, rt, 4 h, 86%; (f) (1) NsCl, pyridine, 88%; (2) Propargylbromide, $K_2CO_3$, DMF, rt, 3 h; then PhSH, rt, overnight, 89%; (g) ethyl bromoacetate, DIEA, DMF, rt, overnight, 86%; (h) $Pd(PPh_3)_4$, CuI, TEA, THF, 60°C, 4 h, 35%; (i) (1) 2N NaOH, dioxane, rt, 3 h; (2) 50% aq. TFA, 0°C to rt, 5 h; (j) PyBOP, DIEA, DMF, rt, overnight, 8% from **7** after HPLC purification.

In addition, we synthesized the truncated ligand **MC1T** to evaluate the contribution of the second adenosine moiety to the inhibitory potency (Scheme 2). Starting from bromide **4**, Sonogashira coupling reaction with ethyl 2-*N*-propargylaminoacetate gave compound **9**. Removal of all protecting groups, followed by cyclization of crude **10** under our previously optimized conditions, resulted in **MC1** in 11% yield from **9**. As observed for compound **8**, rapid degradation of **10** occurred under HPLC purification conditions.

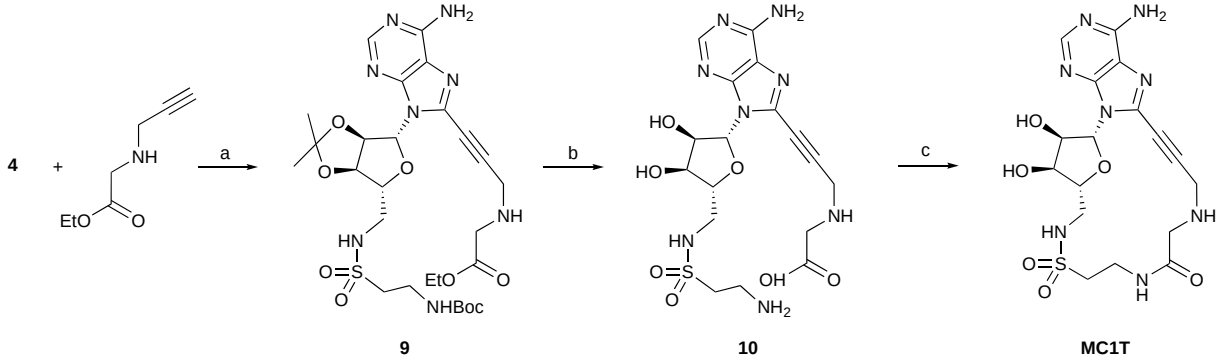


**Scheme 2:** Synthesis of truncated ligand **MC1T**

*Reagents and conditions:* (a) $Pd(PPh_3)_4$, CuI, TEA, THF, 60°C, 4 h, 75%; (b) (1) 2N NaOH, dioxane, rt, 3 h; (2) 50% aq. TFA, 0°C to rt, 5 h; (c) PyBOP, DIEA, DMF, rt, overnight, 11% from **9** after HPLC purification.

*Synthesis of cyclic molecules **MC2** and **MC3***

We previously showed that the functionalization of NKI1 with an alkyl amide at the 5' end has a little impact on the inhibitory activity against *Lm*NADK1 [22]. We thus decided to synthesize two cyclic molecules having an amide bond in place of sulfonamide with two lengths for the linker. The synthetic access is outlined in Scheme 3. Briefly, bromides **11** and **12** were obtained in two steps from **2b** or **2d** by reaction with the appropriate carboxylic acids (*N*-Boc-D-glycine and *N*-Boc-ß-alanine) in the presence of PyBOP and DIEA (Scheme S2). Further Sonogashira coupling reaction with alkyne **6** gave the corresponding diadenosine derivatives **13** and **14**. Removal of protecting groups, followed by cyclization reaction of **15** and **16** under previously optimized conditions, resulted in the formation of **MC2** and **MC3** in 15% and 23% yield, respectively, after HPLC purification.

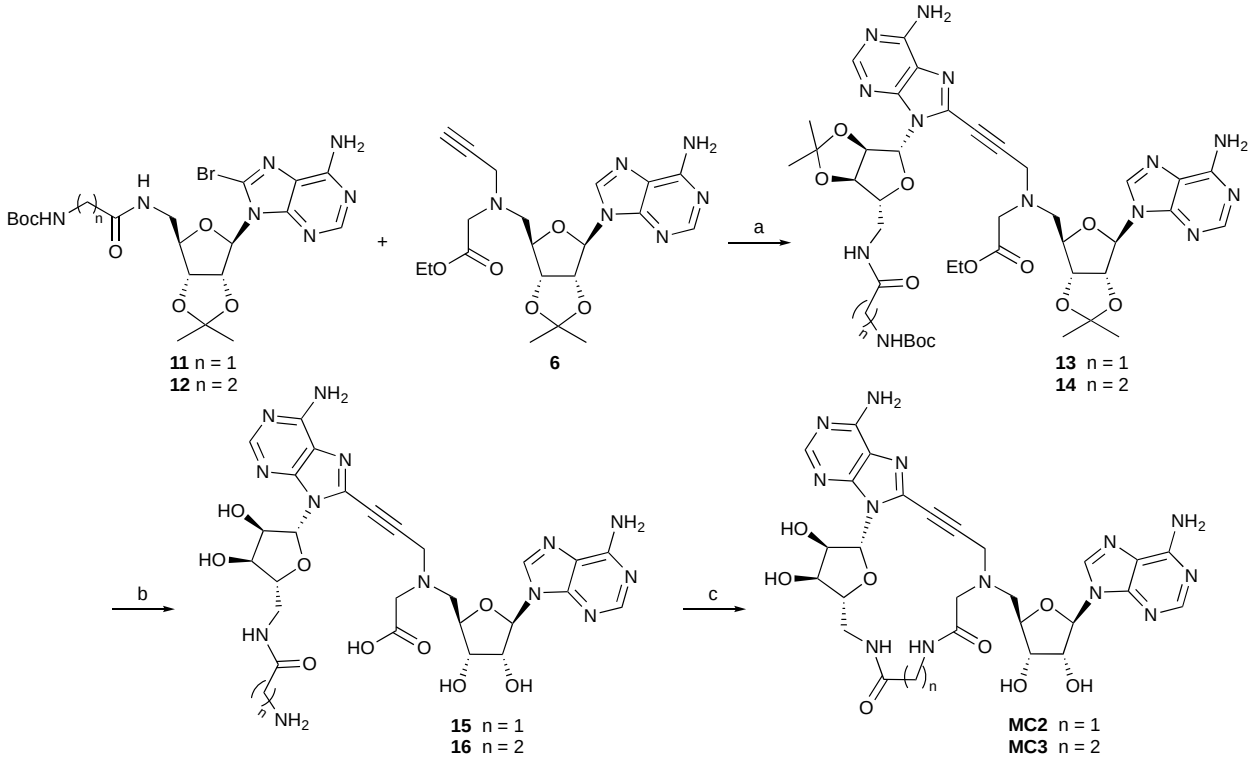


**Scheme 3:** Synthesis of **MC2** and **MC3**
*Reagents and conditions:* (a) $Pd(PPh_3)_4$, CuI, TEA, THF, 60°C, 3 h, 60–35%; (b) (1) 2N NaOH, dioxane, rt, 3 h; (2) 50% aq. TFA, 0°C to rt, 5 h, 75–63%; (c) PyBOP, DIEA, DMF, rt, overnight, 23% from **15** and 15% from **16**, after HPLC purification.

*Synthesis of cyclic compound **MC4***

To evaluate the contribution of the amide bond within the linker to the binding affinity, we synthesized compound **MC4** that contains an inverted amide bond as compared to compound **4** ($CH_2CO$-NH in place of NH-$COCH_2$) while keeping the same ring size. Sonogashira reaction between bromide **17** and alkyne **18**

(prepared as depicted in Scheme S3), followed by deprotection of **19** and PyBOP mediated cyclization reaction of the linear intermediate **20** resulted in **MC4** (Scheme 4).

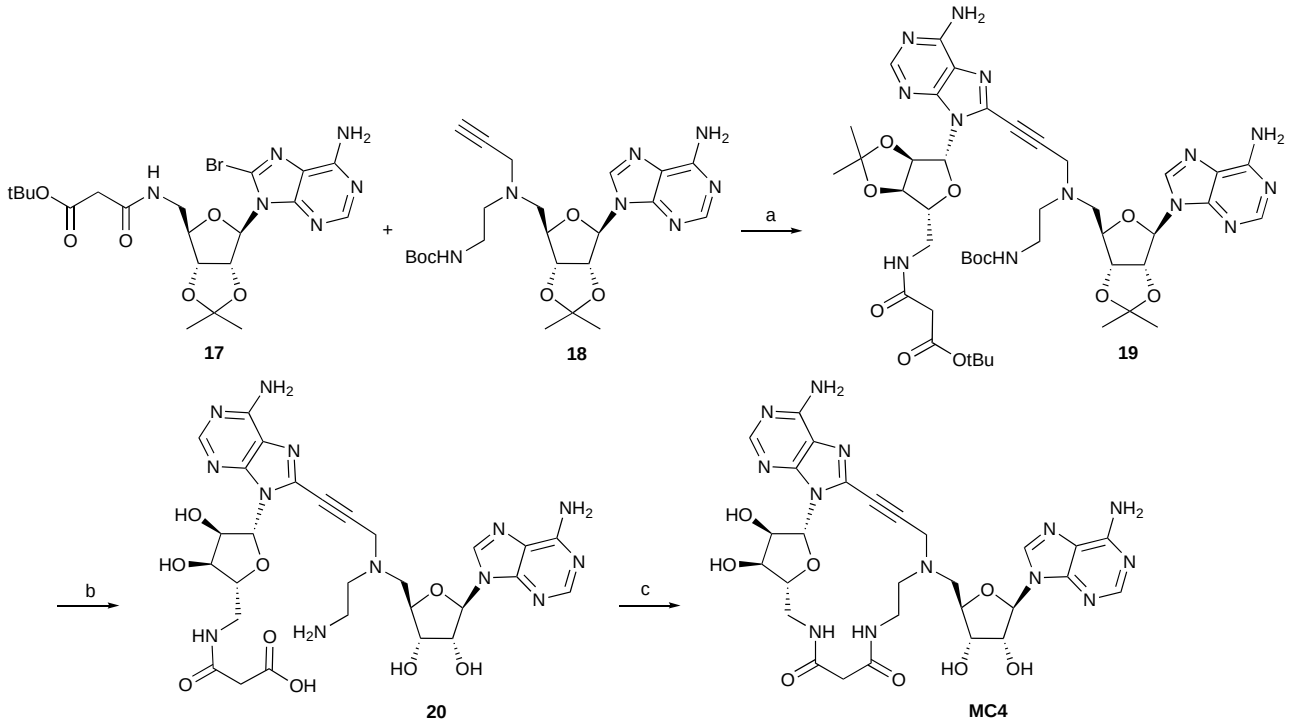


**Scheme 4**: Synthesis of **MC4**

*Reagents and conditions*: a) $Pd(PPh_3)_4$, CuI, $NEt_3$, THF, 60 °C; b) TFA/$H_2O$, 22% in two steps; c) PyBOP, DIEA, DMF, rt, overnight, 8% after HPLC purification.

*Synthesis of cyclic compounds **MC5** and **MC6***

We also synthesized two macrocycles having a 5'-urea functional group, compounds **MC5** and **MC6**, that differ by two carbon atoms within the ring. As outlined in Scheme 5, Sonogashira reaction between alkyne **6** and the urea derivatives **21** or **22** (prepared as depicted in Scheme S4), followed by two-step deprotection of coupling products **23** and **24** afforded the linear intermediates **25** and **26** which were further submitted to PyBOP mediated cyclization reaction into **MC5** and **MC6** in 23 and 15% yield, respectively.

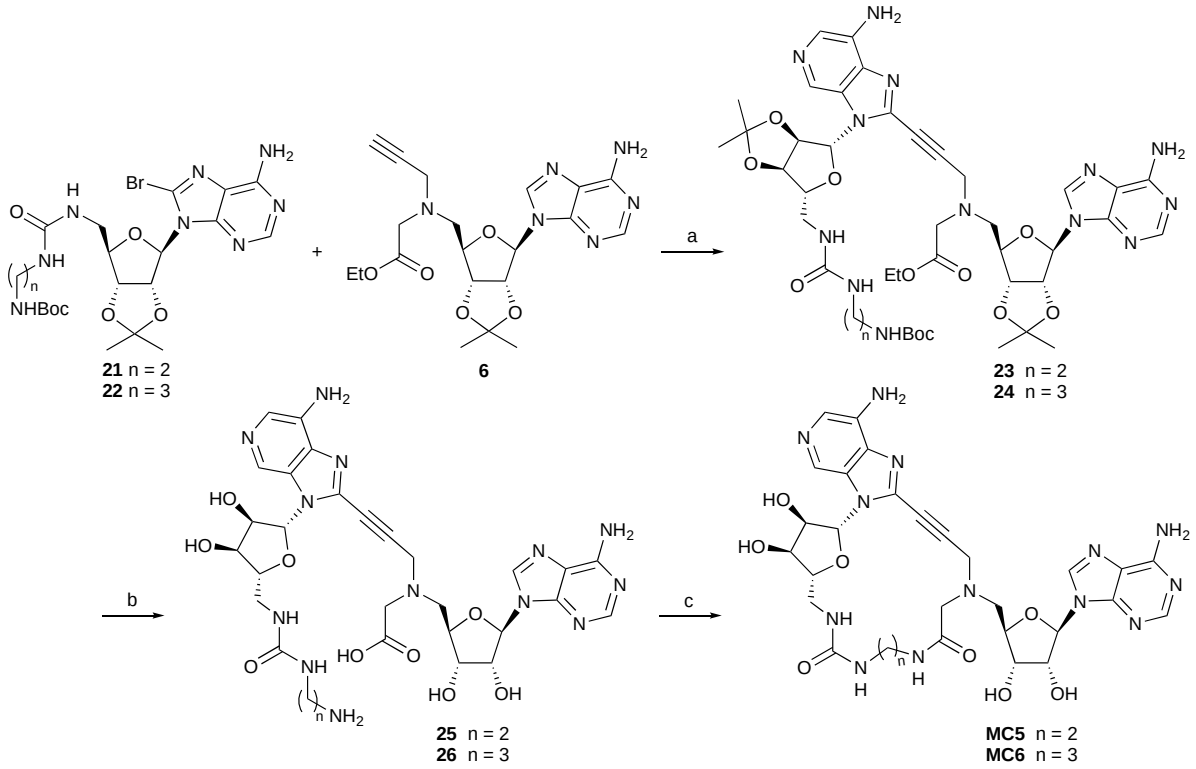


**Scheme 5:** Synthesis of **MC5** and **MC6**
*Reagents and conditions:* (a) $Pd(PPh_3)_4$, CuI, TEA, THF, 60°C, 3 h, 60–35%; (b) (1) 2N NaOH, dioxane, rt, 3 h; (2) 50% aq. TFA, 0°C to rt, 5 h, 75–63%; (c) PyBOP, DIEA, DMF, rt, overnight, 23% from **25** and 15% from **26**.

### 2.4. Effects of MC1-6 on *Lm*NADK1 activity

The inhibitory potency of the synthesized macrocyclic compounds (**MC1-6**, **MC1T)** and the corresponding linear intermediates were determined *in vitro* on recombinant *Lm*NADK1 as described previously [15]. The inhibition efficiency ($K_i$) of macrocycles and their acyclic precursors are compared to that of NKI1, which demonstrated a $K_i$ value of 17 ± 1 µM on *Lm*NADK1 (Table 1).

The best inhibitor was **MC1**, harboring a sulfonamide group, with a $K_i$ of 54 nM. The sulfonamide moiety increased the inhibition efficiency 10-fold compared to the amide containing macrocycle of same length, **MC3** (Table 1). Increasing the length of the linker seems to favor the inhibition as suggested by the comparison of $K_i$ values of **MC2** (linker length of 5 atoms) with **MC3** (6 atoms) or $K_i$ values of **MC5** (7 atoms) with **MC6** (8 atoms). The orientation of the central amide seems to be crucial as suggested by the comparison of the $K_i$ values of **MC3** and **MC4**. The lower inhibition with **MC4** (compared to **MC3**) may be due to the less favorable positioning of this amide bond in the active site of the enzyme (see below). In this series, the most potent inhibitor is the longest one, **MC6** ($K_i$ of 177 nM), suggesting that a too constrained cycle is not so favorable. However, for most compounds, cyclization reaction led to a higher inhibition of *Lm*NADK1 enzymatic activity (Table 1). It should be noted that the absence of the adenosine moiety (truncated MCT1) decreases dramatically the inhibitory activity compared to **MC1** ($K_i$ of MC1T > 125 µM).

**Table 1**: Inhibitory activities of linear intermediates and macrocyclic compounds on *Lm*NADK1 and effect of cyclization expressed as potentiation factor.

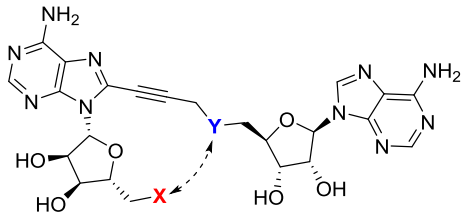

| Ligand | X | Y | $K_i$ *Lm*NADK1[a] (µM) | Cyclization potential (fold) |
|---|---|---|---|---|
| **1** | 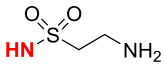 | **O** | 5.5 ± 1.5 | N/A |
| **8** | 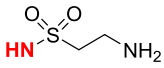 | 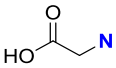 | 91 ± 4 | 1685 |
| **MC1** | 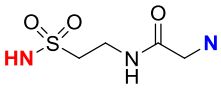 | | 0.054 ± 0.006 | |
| **15** | 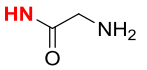 | 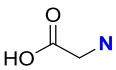 | 104 ± 2 | 6.9 |
| **MC2** | 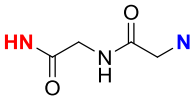 | | 15 ± 2 | |
| **16** | 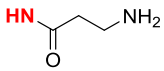 | 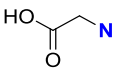 | 19 ± 4 | 38 |
| **MC3** | 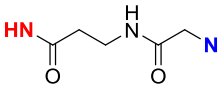 | | 0.504 ± 0.070 | |
| **20** | 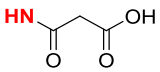 | 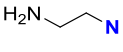 | 53 ± 6 | 7.8 |
| **MC4** | 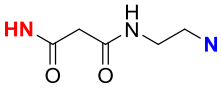 | | 6.8 ± 2.0 | |
| **25** | 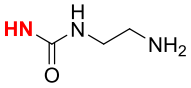 | 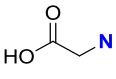 | 18 ± 4 | 2.4 |
| **MC5** | 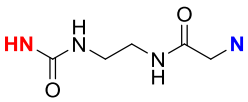 | | 7.6 ± 2.5 | |
| **26** | 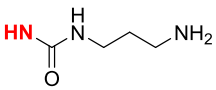 | 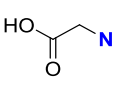 | 16 ± 6 | 90 |
| **MC6** | 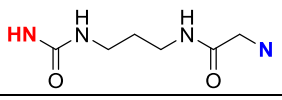 | | 0.177 ± 0.017 | |

[a] Data represent the mean ± standard error of the mean (SEM) values of at least three independent experiments. Compounds were tested at different concentrations chosen on either side of the $K_i$ value.

### 2.5. Effects of compounds MC1-6 on *L. monocytogenes* and *S. aureus* growth

Since most of the macrocyclic compounds had better inhibitory potency on recombinant NADKs than NKI1, we next evaluated their ability to affect growth of *L. monocytogenes* and *S. aureus in vitro*. As previously reported [15], growth of *S. aureus* was inhibited by NKI1 or levofloxacin (Figure 4A). However, no significant growth reduction was observed upon treatment with the macrocyclic compounds. Similarly, while *L. monocytogenes* growth was severely impaired by levofloxacin, it was not significantly affected by macrocyclic compounds (Figure 4B). Of note, NKI1 did not inhibit growth of *L. monocytogenes*. Together, these results indicate that while displaying better inhibitory properties on recombinant NADKs, the macrocyclic compounds fail to inhibit bacterial growth *in vitro* in our experimental conditions.

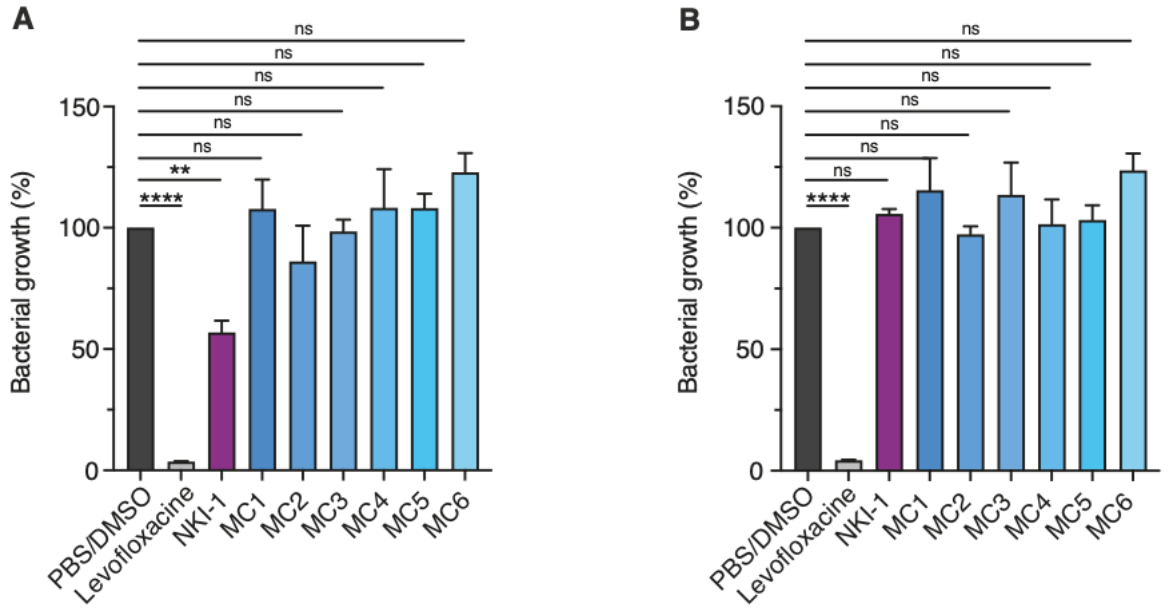


**Figure 4:** Macrocyclic compounds do not affect growth of *S. aureus* or *L. monocytogenes in vitro*.
A) Percentage of *S. aureus* growth after 6h of culture in BHI broth at 37°C supplemented with PBS/10% DMSO, 10 µg/mL levofloxacin, 0.01 µg/mL NKI1 or macrocyclic compounds. Bars indicate the standard errors of the means of biological replicates (n=6). Comparison of data was performed using one-way analysis of variance (****$p < 0.0001$, **$p < 0.01$, ns: non-significant). B) Percentage of *L. monocytogenes* growth after 6h of culture in BHI broth at 37°C supplemented with PBS/1% DMSO, 10 µg/mL levofloxacin, 0.01 µg/mL NKI1 or macrocyclic compounds. Bars indicate the standard errors of the means of biological replicates (n=6). Comparison of data was performed using one-way analysis of variance (****$p < 0.0001$, ns: non-significant).

Since deficient bacterial cell penetration could mask antibacterial activity of compounds targeting cytoplasmic targets, we next determined the effect of **MC1-6** on growth of *L. monocytogenes* and *S. aureus in vitro* in presence of membrane permeabilizing polymyxin B. Interestingly, *S. aureus* was sensitized to the 6 macrocyclic compounds when incubated with 40 µg/mL polymyxin B (Figure S1). In contrast, **MC1-6** were not active against *L. monocytogenes* irrespective of the concentration of polymyxin tested (Figure S2).

These results suggest that limited access to the target, along with other factors, could contribute to some extent to the absence of activity of macrocycles in our experimental conditions.

**2.6. X-ray structures of *Lm*NADK1 bound to macrocyclic compounds**

The crystal structures of 12 distinct complexes with *Lm*NADK1 were solved and refined to 1.54–2.41 Å resolution (Table S1, Figure 5). Most of these structures were solved after ligand soaking into preformed *Lm*NADK1 crystals. Surprisingly, we could not obtain the crystal structure in complex with the best compound **MC1**, using the same strategy as for the other macrocycles. Instead, a co-crystallization followed by an additional soaking was necessary to solve the structure of this particular complex (Figure 5B). Nevertheless, **MC1** is accommodated in a very similar fashion as the other compounds and especially **MC3** in agreement with their shared length.

These structures provided insight into the precise conformation of six linear precursors and their corresponding macrocycles (Figure 5A-L). First, the two adenosine moieties occupied the same positions as previously observed for other inhibitors such as NKI1. Of note, the whole molecules were clearly visible in the electron densities including the most flexible parts of the linear compounds but for the very terminal amino groups.

In most of the linear compounds (numbered **8**, **15**, **16**, **25** and **26**) the carboxylic acid attached to the *N*-propargyl moiety points toward the solvent and the groove made by the glycine G43 and histidine H223 (which is frequently flipped out in these structures). The amino alkyl chain at the same position in compound **20** points also outward and in the same groove (Figures 5G). The linear precursors of the urea and amide series showed a similar orientation stabilized by one or two hydrogen bonds with the neighboring ribose moiety but for the compound **15** (see Figures 5 and S3A and S3C). In this particular case, the hydrogen bond involved, instead, the amino atom of the propargyl linker. Meanwhile, the short amino alkyl chains differ and point into distinct conformations but the locally weaker electron densities suggest some flexibility. The unique sulfonamide precursor **8** showed a distinct orientation of its 5' extension compared to the other linear compounds, with no hydrogen bond to the second ribose (nor the propargyl nitrogen atom).

The newly formed macrocycles were clearly visible in all the crystal structures in agreement with conformation constraints created by the additional covalent bond and the rigid amide, urea and/or sulfonamide groups present along the short connectors.

Interestingly, it is not the longest ones that showed the major rearrangements upon macrocyclization (see Figures S3 and S4). Indeed, shorter macrocycles led to some reorientation even for the group directly attached to the 5' end. This feature indicates that in some cases, some of the conformation constraints were too strong to be compatible with the good intra- or inter-molecular interactions observed in the linear precursors (such as the hydrogen bonds to the ribose moiety). This is illustrated by the position of the

amide group in **MC2** (compared to its linear precursor **15**). In the linear precursor **15**, a weak internal hydrogen bond involves the nitrogen atom of the 5' amide group with the nitrogen atom of the propargyl linker (distance 3.5 Å). In the macrocycle **MC2**, this hydrogen bond is broken and substituted by a slightly shorter one (3.4 Å) between the amide nitrogen and the oxygen atom O4' of the second ribose (Figures 5C and 5D). Still, macrocyclization improves affinity 7-fold in that case. Another type of rearrangement is observed upon macrocyclization of compound **16** into **MC3** (Figures 5E and 5F). In both compounds, the oxygen atom O4' from the second ribose is involved in two hydrogen bonds but either with the nitrogen atom the 5' amide group (distances: 3.1 Å and 3.4 Å in compound **16**) or the nitrogen atom of the newly form amide group (distances: 3.1 Å and 2.7 Å in **MC3**). Overall, this macrocyclization brings a 40-fold improvement. In the macrocycle **MC4**, which harbors an inverted amide group (compared to **MC3**), only one hydrogen bond is kept, and the inverted amide group does not bring any favorable interactions (either with the protein or intramolecularly). In this series, the increase in efficacy seems to correlate with some strengthening of the hydrogen bond network.

In the urea-based series, the shortest macrocycle, **MC5**, shows a constrained conformation preventing any hydrogen bond involving the urea while its linear precursor did form such a hydrogen bond to the O4' oxygen of the second ribose. This macrocyclization to **MC5**, with the second longest linker, yields a very modest gain in potency of 2.4. One the contrary, in the one-carbon longer macrocycle **MC6**, the closed chain and its linear version adopts a similar conformation. In both inhibitors (Figures 5K and 5L), two similar hydrogen bonds are formed between the urea nitrogen atoms and the O4' oxygen of the second ribose (distances 3.4 Å and 3.3 Å in **MC6** instead of 3.0 Å and 2.9 Å in compound **26**). In addition, favorable van der Waals contacts (distances: 3.8 Å and 3.9 Å) between two carbon atoms of the linking alkyl chain and the adenine of the second adenosine (Figure 5L) can be observed. Of note, the one-atom shorter **MC5** showed no such contact (Figure 5J). Hence, proper orientation of the urea group seemed to require a slightly longer alkyl chain of 3 carbon atoms instead of 2. While shorter macrocycles were expected to provide higher entropy gain, local constraints due to rigid groups along the closed chain (e.g.: urea, amide) led to counterintuitive results. The lower gain in potency were mainly associated with the loss of intramolecular interactions (mostly hydrogen bonds).

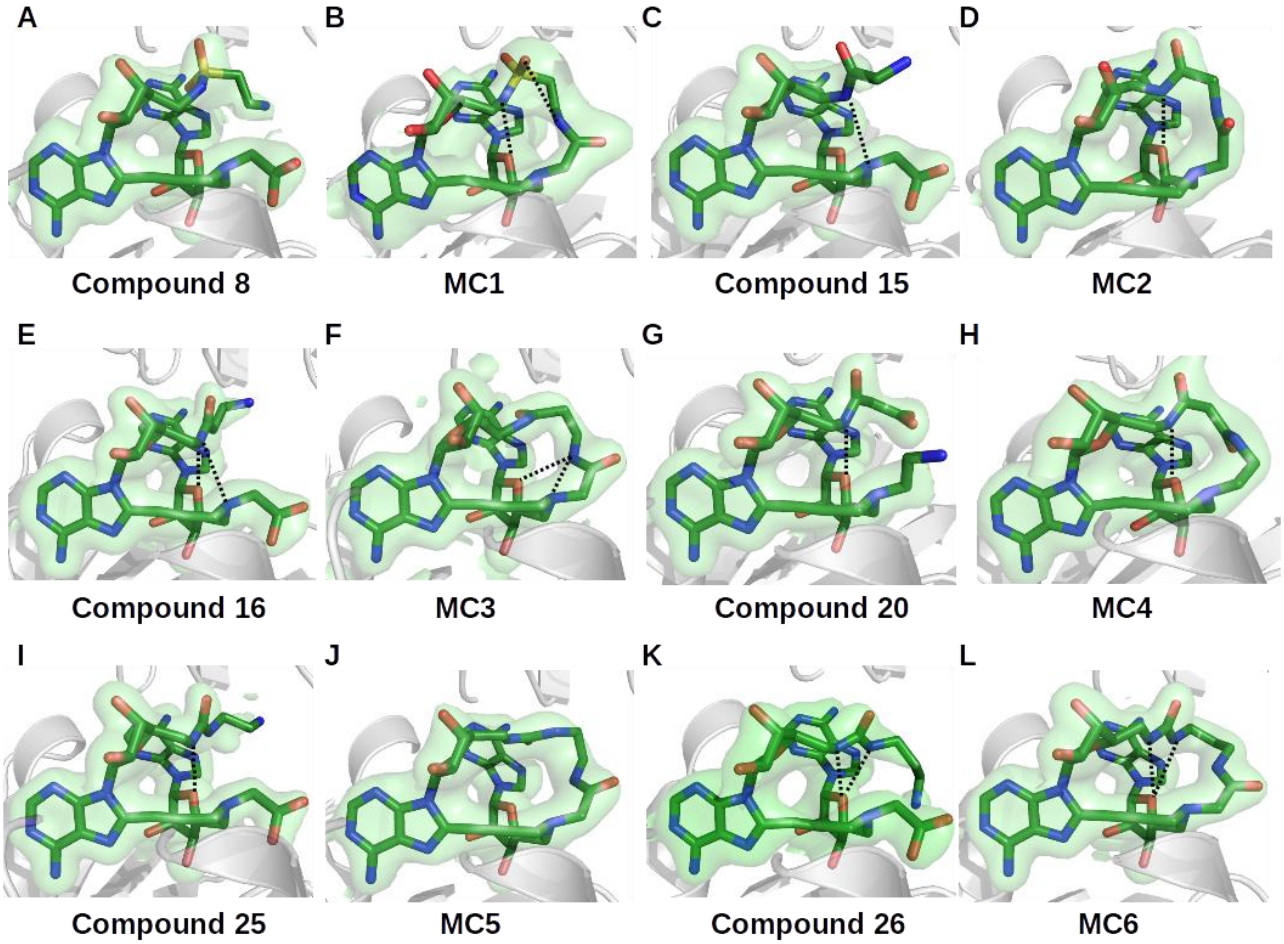


**Figure 5: Crystal structures of linear precursors and corresponding macrocycles bound to *Lm*NADK1**.
(A-L) Macrocycles **MC1-6** and their precursors are shown as sticks in CPK colors (with green carbons) in the active site of *Lm*NADK1. The protein is drawn as grey ribbons. The electron density is shown as a green surface around the ligand, which is the view of the 2Fo−Fc electron density map contoured at 0.9 σ. Black dashed lines indicate intramolecular hydrogen bonds. The figures were drawn using Pymol (www.pymol.org).

Finally, we analyzed the conformation of **MC1**, the best NADK inhibitor ever described so far (54 nM), while its precursor is one of the weakest inhibitors described here (0.09 mM). The linear and open compound **8** showed no internal hydrogen bond and no compensatory interaction with the protein in agreement with its poor activity. On the contrary, the circular inhibitor **MC1** showed a conformation stabilized by two intramolecular hydrogen bonds. One hydrogen bond involved an oxygen atom of the sulfonamide group and the nitrogen of the newly formed amide. Meanwhile, the nitrogen atom of the sulfonamide group is oriented toward the O4' of the second ribose moiety and forms a second hydrogen bond. This partially resembles the situation observed in second best inhibitor, **MC6**, which harbors a urea group and a two-atom longer linker. Of note, the two oxygen atoms of the sulfonamide do not attract a nearby arginine (R148) that also showed no contact with the carbonyl in *Lm*NADK1-**MC6** complex. Therefore, the better

affinity of **MC1** over **MC6** and the other macrocycles would be explained by an internal hydrogen bond between the nitrogen atom of the closing amide and an oxygen atom of the sulfonamide group (Figure 5B). The sulfonamide group may also be more constrained than the planar urea and this could bring extra entropy gain for its bound conformation. This would contribute to the 9-fold improvement in potency over the compound **MC3** of identical length.

While the compounds showed no detectable activity on whole *L. monocytogenes* bacteria, some activity were detected against *S. aureus* in presence of polymyxin B. However, ranking of the macrocyclic compounds differs in this assay and in the enzymatic inhibition performed on purified *Lm*NADK1 (SaNADK could not by purified to homogeneity in our hands). Although it might come from some distinct solubility and permeability properties, it might arise also from some variations (T133 and F193 instead of P132 and Y192) in the active site of *Sa*NADK compared to that of LmNADK1. Indeed, one substitution, T133, brings a polar residue in the vicinity of one amide group within the macrocyclization chain. The hydroxyl of the side chain of T133 may form a hydrogen bond with a carbonyl oxygen of this amide group. This could account for the (slightly) better activity of **MC2**, **MC3** and **MC5** against *S. aureus* compared to that of **MC1** and **MC6**, the two most potent inhibitors of *Lm*NADK1. This particular feature may be further exploited to improve the specificity and the potency against staphylococcal NADKs.

## 3. Conclusion

New compounds were designed from the various crystal structures of linear diadenosine derivatives bound to *Lm*NADK1, synthesized, and tested *in vitro* against this still orphan drug target. A series of adenosine-based macrocyclic compounds were successfully obtained through ring closure reaction involving an amide bond formation. The acyclic precursors that contained the complementary functional groups (carboxylic acid and amine) were designed to minimize the building blocks required for generating these 16- to 19-membered rings. The macrocycles were formed from unprotected precursors by intramolecular amide bond formation and isolated in acceptable yields (ranging from 8 to 23% depending on the nature of the linking chain). Macrocycles **MC1-6** and acyclic precursors were tested *in vitro* as inhibitors of recombinant NADK from *L. monocytogenes* (*Lm*NADK1). Macrocyclization was shown to improve the potency against the purified enzyme with up to a 1685-fold improvement in affinity (**MC1** versus **8**). The 55 nM active compound **MC1** (a 10,000 better binder than NAD) represents a novel and promising inhibitor of NADK, the tightest binder described to date. Crystal structures explain the stabilizing features provided by the new linkers. This will help guiding the design of compounds also efficient *in vivo*.

The resulting macrocycles appeared inactive *in vitro* against the two pathogenic Gram (+) bacteria, *L. monocytogenes* and *S. aureus*, which express a similar NADK. We cannot exclude lower affinity for the *Sa*NADK, although, comparative docking suggested no major issue. Instead, solubility and cell penetration could be important issues to solve to turn such compounds into new drugs. Indeed, activity of **MC1-6** could

be revealed by treatment of *S. aureus* with membrane permeabilizing polymyxin B. In contrast, **MC1-6** were not active against *L. monocytogenes* in presence of polymyxin B. Several factors could account for this difference, such as specific envelop composition, metabolic properties and presence of a second NADK in *L. monocytogenes.* Vectorization or other strategies to improve their cell penetration will be implement in the future to fully benefit for their potent inhibition of the NADKs from Gram (+) pathogens [36-38].

The observed conformations of these new inhibitors and the orientation of the surrounding residues provide new information in order to derive additional chemical modifications to improve further this chemical series. While considered as highly promising for improve pharmacological properties and inhibitory potencies, macrocycles are still seldom characterized structurally and too few examples have been described at atomic details despite seminal examples (see [39] for macrocyclic natural products) and now some protein-kinase inhibitors [29,31]. This study also revealed, in very precise details, the contradicting constraints in the design of macrocycles and the difficulties to anticipate the outcome of ring closure. This should be very helpful for the design of potent ligands beyond the scope of the NADK inhibition and it may constitute an interesting gold standard to calibrate theoretical methodologies dedicated to drug design by macrocyclization.

## 4. Materials and methods

### 4.1. Structure-based design of novel cyclic diadenosines

Virtual molecules were designed by derivation from the compound NKI1. 3D conformers were generated from SMILE strings using Grade (http://grade.globalphasing.org/). The resulting compounds were docked in the electron density of NKI1 and minimized in various conformations compatible with the environment using COOT [40]. Virtual docking was also performed using PLANTS [41]. The results were compared to extract the most plausible conformations. Interactions with the neighboring residues were analyzed and some reorientations of nearby side-chains were also modeled. From this focused screen, a selection of optimal paths for connecting the two 5’ ends of our di-adenosine lead-compound were scrutinize for synthetic feasibility.

### 4.2. X-ray structures of LmNADK1 bound to cyclic compounds

The soaking procedure described previously [15] was used to get crystals of the target bound to the synthesized macrocycles **MC2-6**. For **MC1**, direct soaking failed and instead co-crystallization at alkaline pH was attempted and showed partial occupancy of the macrocycle into the active site. Full occupancy was achieved by soaking more compound prior to mounting and freezing the corresponding crystals. The X-ray structures were solved by molecular replacement using PDB ID 6RGC [15] as a starting template and refined to 2.2–2.4 Å resolution using the software Phenix [42]. Manual rebuilding in the electron densities were

performed in COOT [40]. A few rounds of optimization rapidly led to convincing refinements for all the structures.

### 4.3. Chemistry

*4.3.1. Chemicals and General Methods*

Commercially available reagents and solvents, unless otherwise stated, were purchased from commercial suppliers, and used as received. All air and water sensitive reactions were carried out under an *argon* atmosphere. Analytical thin-layer chromatography (TLC) was performed on TLC plates pre-coated with silica gel 60 $F_{254}$. Compounds were visualized with UV light (254 nm) and by spraying with a mixture of ethanol/anisaldehyde/sulfuric acid/acetic acid (90/5/4/1), followed by heating. Reactions were also monitored using an HPLC system (Agilent 1200 equipped with a C18 reverse phase column) coupled to a mass spectrometer (ESI source). Flash chromatography was performed with silica gel 60 (230–400 mesh). HPLC purification was carried out on an Agilent system (1100 Series) equipped with a diode array detector using a C18 reverse phase column (Kromasil, 5 µm, 100 Å, 250×10 mm) and a linear gradient of acetonitrile in 10 mM triethylammonium acetate (TEAA) buffer over 15 or 20 min at a flow rate of 4 mL/min. Retention time ($t_R$) and gradient are specified. NMR spectra were recorded on Bruker Avance 400 ($^1$H at 400.13 MHz and $^{13}$C at 100.62 MHz). Chemical shifts ($\delta$) are reported in parts per million (ppm) relative to the solvent signals. Coupling constants (*J* values) are reported in Hz and splitting patterns are indicated as follows: s = singlet, d = doublet, t = triplet, q = quartet, p = pentet, m = multiplet, br = broad signal. The complete assignment of $^1$H and $^{13}$C signals was performed by analysis of the correlated homonuclear $^1$H,{$^1$H}–COSY and heteronuclear $^1$H,{$^{13}$C}–HMBC, $^1$H,{$^{13}$C}–HSQC spectra. High-resolution mass spectra (HRMS) were recorded with a Q-Tof Micro mass spectrometer under electrospray ionization in positive ionization mode using a mobile phase of acetonitrile/water with 0.1% formic acid. The purity of all tested compounds was greater than 97% as determined using NMR spectroscopy and HPLC analysis (C18 Kromasil) using a linear gradient of acetonitrile in 10 mM TEAA buffer over 15 or 20 min at a flow rate of 1 mL/min.

Synthetic procedures for intermediate building blocks (outlined in Scheme S1-S4) and compounds **MCT1**, **MC2**, **MC3**, **MC4** and **MC5** are included in Supplementary information. Synthesis of **MC1** and **MC6** is given below.

*4.3.2. Synthesis of **MC1***

**5'-(2-*N*-Boc-aminoethylsulfonyl)amino-5'-deoxy-2',3'-*O*-isopropylidene-8-bromo-adenosine (4)**

To a solution of **3c** (0.60 g, 1.17 mmol) in a mixture of dioxane/acetate buffer pH 5.3 (8.2 mL/4.7 mL) was slowly added dropwise bromine (0.12 mL, 2.34 mmol). After stirring for 4 h at room temperature, the reaction was quenched by addition of saturated aqueous solution of $Na_2S_2O_3$ and the mixture was

extracted with ethyl acetate (2 x 100 mL). The combined organic phases were washed with aqueous NaCl (20 mL), dried over $Na_2SO_4$, filtered and concentrated under reduced pressure. The crude product was purified by flash column chromatography (30 g $SiO_2$, 3% MeOH in DCM) to give **4** (0.60 g, 86%). $^1$H NMR (400 MHz, DMSO-$d_6$): $\delta$ 1.34 (s, 3H, $CH_3$ isop), 1.35 (s, 9H, $CH_3$ Boc), 1.56 (s, 3H, $CH_3$ isop), 3.05-3.11 (m, 2H, $SCH_2$), 3.12-3.30 (m, 4H, $NCH_2$, H-5' and H-5''), 4.22-4.29 (m, 1H, H-4'), 5.10 (dd, *J* = 2.9 Hz, *J* = 6.3 Hz, 1H, H-3'), 5.62 (dd, *J* = 2.5 Hz, *J* = 6.3 Hz, 1H, H-2'), 6.04 (d, *J* = 2.5 Hz, 1H, H-1'), 6.80 (br t, 1H, NHBoc), 7.55 (br, 2H, $NH_2$), 7.61 (br, 1H, NH), 8.14 (s, 1H, H-2); $^{13}$C NMR (100 MHz, DMSO-$d_6$): $\delta$ 25.66 and 27.50 ($CH_3$ isop), 28.60 (3C, $CH_3$ Boc), 35.47 ($NCH_2$), 44.51 (C-5'), 51.10 ($SCH_2$), 78.56 (Cq tBu), 82.34 (C-3'), 82.79 (C-2'), 86.07 (C-4'), 91.47 (C-1'), 113.91 (Cq isop), 119.79 (C-5), 126.65 (C-8), 150.08 (C-4), 153.28 (C-2), 155.54 (C-6), 155.78 (CO); HRMS (ESI-TOF): *m/z* calcd for $[C_{20}H_{30}BrN_7O_7S+H]^+$ 592.1189 and 594.1171, found 592.1195 and 594.1197.

**Ethyl *N*-propargyl-*N*-(5'-deoxy-2',3'-*O*-isopropylidene-adenosinyl)glycinate (6)**

To a stirred solution of **5** (0.34 g, 1.0 mmol) in DMF (5 mL) were added DIEA (0.52 mL, 3.0 mmol) and ethyl bromoacetate (0.17 mL, 1.5 mmol). After stirring overnight at room temperature, volatiles were removed under reduced pressure and the residue purified by flash column chromatography (35 g $SiO_2$, 3 to 3.5 % MeOH in DCM) to give **6** (0.37 g, 86%). $^1$H NMR (400 MHz, $CDCl_3$): $\delta$ 1.25 (t, *J* = 7.0 Hz, 3H, $CH_3$), 1.40 (s, 3H, $CH_3$), 1.63 (s, 3H, $CH_3$), 2.19 (t, *J* = 2.4 Hz, 1H, HC≡), 2.92 (dd, *J* = 6.9 Hz, *J* = 13.7 Hz, 1H, H-5'), 2.98 (dd, *J* = 1.7 Hz, *J* = 7.1 Hz, 1H, H-5''), 3.42 (s, 2H, $CH_2$), 3.57 (d, *J* = 2.3 Hz, 1H, $CH_2$-C≡), 4.15 (dq, *J* = 3.7 Hz, *J* = 3.7 Hz, 2H, $CH_2$), 4.37-4.44 (m, 1H, H-4'), 5.10 (dd, *J* = 3.7 Hz, *J* = 6.5 Hz, 1H, H-3'), 5.44 (dd, *J* = 2.4 Hz, *J* = 6.5 Hz, 1H, H-2'), 5.81 (br, 2H, $NH_2$), 6.11 (d, *J* = 2.4 Hz, 1H, H-1'), 8.00 (s, 1H, H-8), 8.37 (s, 1H, H-2); $^{13}$C NMR (100 MHz, $CDCl_3$): $\delta$ 14.14 ($CH_3$), 25.44 and 27.17 ($CH_3$ isop), 43.73 (***C***$H_2$-C≡), 53.98 and 55.37 (C-5' and $NCH_2CO$), 60.59 ($OCH_2$), 73.45 (H***C***≡), 78.41 (HC≡***C***), 82.70 (C-3'), 83.91 (C-2'), 85.63 (C-4'), 90.45 (C-1'), 114.52 (Cq isop), 120.26 (C-5), 139.85 (C-8), 149.44 (C-4), 153.11 (C-2), 155.61 (C-6), 170.61 (CO); HRMS (ESI-TOF) *m/z* calcd for $[C_{20}H_{26}N_6O_5+H]^+$ 431.2043, found 431.2058.

**5'-Deoxy-5'-[*N*-(3-(5'-deoxy-5'-(2-Boc-aminoethyl)sulfonamido-2',3'-*O*-isopropylidene-adenosin-8-yl)prop-2-yn-1-yl)-2-(ethyl ethanoate)amino]-2',3'-*O*-isopropylidene-adenosine (7)**

To a solution of alkyne **6** (0.33 g, 0.76 mmol) and bromide **4** (0.59 g, 1.0 mmol) in THF (8 mL) was added triethylamine (0.32 mL, 2.28 mmol). The reaction mixture was degassed with argon (3 times) before adding CuI (15 mg, 10 mol%) and $Pd(PPh_3)_4$ (46 mg, 5 mol%) followed by argon degassing (3 times). After stirring for 4 h at 60 °C, volatiles were removed and the residue was purified by two successive flash column chromatography (40 g $SiO_2$, 2 to 6% MeOH in DCM; 25 g $SiO_2$, 0 to 6% MeOH in ethyl acetate) to give **7** (0.25 g, 35%). $^1$H NMR (400 MHz, DMSO-$d_6$): $\delta$ 1.17 (t, *J* = 7.3 Hz, 3H, $CH_3$), 1.30 (s, 3H, $CH_3$ isop), 1.33 (s, 3H, $CH_3$ isop), 1.34 (s, 9H, $CH_3$ Boc), 1.48 (s, 3H, $CH_3$ isop), 1.54 (s, 3H, $CH_3$ isop), 2.85 (dd, *J* = 6.6 Hz, *J* = 13.5 Hz, 1H,

H-5'b), 2.96 (dd, *J* = 6.7 Hz, *J* = 13.5 Hz, 1H, H-5"b), 3.07-3.13 (m, 2H, $CH_2$), 3.15-3.33 (m, 4H, $CH_2$, H-5'a and H-5”a), 3.48 (ABq, *J* = 17.0 Hz, 2H, $NCH_2CO$), 3.93 (br, 2H, $CH_2$-C≡), 4.03 (q, *J* = 7.1 Hz, 2H, $CH_2$ OEt), 4.04-4.10 (m, 2H, $CH_2$), 4.25 (td, *J* = 2.7 Hz, *J* = 5.7 Hz, 1H, H-4'a), 4.34 (td, *J* = 3.2 Hz, *J* = 6.3 Hz, 1H, H-4'b), 5.05 (dd, *J* = 2.9 Hz, *J* = 6.4 Hz, 1H, H-3'a), 5.08 (dd, *J* = 3.1 Hz, *J* = 6.4 Hz, 1H, H-3'b), 5.46-5.52 (m, 2H, H-2'a and H-2'b), 6.13 (d, *J* = 2.8 Hz, 1H, H-1'a), 6.14 (d, *J* = 2.6 Hz, 1H, H-1'b), 6.80 (br t, 1H, NHBoc), 7.30 (s, 2H, $NH_2$), 7.60 (s, 2H, $NH_2$), 7.70 (br t, 1H, NH), 8.15 (s, 1H, H-2b), 8.18 (s, 1H, H-2a), 8.32 (s, 1H, H-8b); $^{13}$C NMR (100 MHz, DMSO-$d_6$): $\delta$ 14.44 ($CH_3$ OEt), 25.64 and 25.71 ($CH_3$ isop), 27.44 (2C, $CH_3$ isop), 28.58 (3C, $CH_3$ Boc), 35.48 ($CH_2$NBoc), 44.00 (***C***$H_2$-C≡), 44.53 (C-5'a), 51.03 ($SCH_2$), 55.21 and 55.35 (C-5'b and N***C***$H_2CO$), 60.55 ($CH_2$ OEt), 74.37 (***C***≡C-$CH_2$), 78.56 (Cq tBu), 82.26, 82.89 and 83.24 (C-2'a, C-2'b, C-3'a and C-3'b), 84.52 (C-4'b), 85.56 (C-4'a), 89.57 (C-1'b), 89.97 (C-1'a), 92.93 (C≡***C***-$CH_2$), 113.86 and 113.96 (Cq isop), 119.35 and 119.67 (C-5a and C-5b), 132.87 (C-8a), 140.424 (C-8b), 148.50 and 149.27 (C-4a and C-4b), 153.16 and 154.15 (C-2a and C-2b), 155.77 (CO Boc), 156.52 and 156.61 (C-6a and C-6b), 170.48 (CO); HRMS (ESI-TOF) m/z calcd for [$C_{40}H_{35}N_{13}O_{12}S$+H] 942.3887, found 942.3879.

**5'-Deoxy-5'-[*N*-(3-(5'-deoxy-5'-(2-aminoethyl)sulfonamido-adenosin-8-yl)prop-2-yn-1-yl)-2-(acetic acid)amino]-adenosine (8)**

To a suspension of **7** (235 mg, 0.25 mmol) in water (1.25 mL) and 1,4-dioxane (1.25 mL) was added NaOH (2N in water, 250 µL, 0.5 mmol). After 6 h at room temperature, volatiles were removed by lyophilization and the residue was treated by an ice cooled TFA solution (70% in water, 2.0 mL). After 4 h at room temperature, water was added and the reaction mixture was lyophilized. The crude product **8** was used without further purification in the next step. HRMS (ESI-TOF) m/z calcd for [$C_{27}H_{35}N_{13}O_{10}S$+H] 734.2423, found 734.2414.

**Macrocycle MC1**

A solution of crude **8** (60% portion from **7**, 0.15 mmol) in DMF (37 mL) was added dropwise over 2.5 h to a solution of PyBOP (117 mg, 0.225 mmol) and DIEA (156 µL, 0.90 mmol) in DMF (2 mL). After 12 h at room temperature, a solution of PyBOP (78 mg, 0.225 mmol) and DIEA (52 µL, 0.90 mmol) in DMF (1 mL) was added to the mixture. When the reaction was judged nearly complete (LC-MS analysis), volatiles were removed under reduced pressure and the residue was purified by reverse phase HPLC (5–20% acetonitrile in 10 mM TEAA buffer, linear gradient over 15 min, $t_R$ = 11.4 min) to yield **MC1** (7 mg, 8%). $^1$H NMR (400 MHz, DMSO-$d_6$): $\delta$ 2.92-3.13 (m, 2H, H-5'b and H-5"b), 3.15-3.50 (m, 6H, 2 $CH_2$, H-5'a and H-5”a), 3.81 (ABq, 2H, $CH_2$-C≡), 3.88-3.95 (m, 1H, H-4'a), 4.08-4.20 (m, 3H, H-4'b, H-3'b and H-3'a), 4.66 (q, *J* = 5.1 Hz, 1H, H-2'), 4.84 (dd, *J* = 5.8 Hz, 1H, H-2'), 5.27 (d, *J* = 5.3 Hz, 1H, OH-3'), 5.34 (d, *J* = 5.2 Hz, 1H, OH-3'), 5.48 (d, *J* = 6.0 Hz, 1H, OH-2'), 5.55 (d, *J* = 5.8 Hz, 1H, OH-2'), 5.91 (d, *J* = 4.9 Hz, 1H, H-1'), 6.08 (d, *J* = 6.1 Hz, 1H, H-1'), 7.25 (s, 2H, $NH_2$), 7.32 (br t, 1H, NH-5'), 7.57 (s, 2H, $NH_2$), 8.00 (t, 1H, NH), 8.17 (s, 1H, H-2), 8.19 (s, 1H, H-2), 8.39

(s, 1H, H-8b); $^{13}$C NMR (100 MHz, DMSO-$d_6$): $\delta$ 34.57 ($CH_2N$), 44.56 (***C***$H_2$-C≡), 45.31 (C-5'a), 51.38 ($CH_2$), 57.31 (C-5'b), 57.83 ($CH_2$), 71.33, 71.84, 72 32 and 73.17 (C-3'a, C-3'b, C-2'a, C-2'b), 75.77 (***C***≡C-$CH_2$), 82.85 (C-4'b), 84.84 (C-4'a), 87.87 (C-1'), 88.35 (C-1'), 92.84 (C≡***C***-$CH_2$), 118.74 and 119.61 (C-5a and C-5b), 131.86 (C-8a), 140.27 (C-8b), 149.80 and 150.06 (C-4a and C-4b), 153.16 and 154.50 (C-2a and C-2b), 156.26 and 156.50 (C-6a and C-6b), 170.25 (CO); HRMS (ESI-TOF) m/z calcd for [$C_{27}H_{33}N_{13}O_9S$+H] 716.2318, found 716.2305.

*4.3.3. Synthesis of **MC6***

**5'-Deoxy-5'-[*N*-(3-(5'-deoxy-5'-(3-(3-*N*-Boc-aminopropyl)ureido)-2',3'-*O*-isopropylidene-adenosin-8-yl)prop-2-yn-1-yl)-2-(ethyl ethanoate)amino]-2',3'-*O*-isopropylidene-adenosine (24)**

To a solution of alkyne **6** (123 mg, 0.29 mmol) and bromide **22** (251 mg, 0.43 mmol) in THF (9.0 mL) was added triethylamine (120 µL, 0.86 mmol). The reaction mixture was degassed with argon for 15 minutes before adding sequentially CuI (5 mg, 10 mol%) and $Pd(PPh_3)_4$ (17 mg, 5 mol%) followed by a second 15 minutes argon degassing. After 16 h at 60 °C, volatiles were removed and the residue was purified by flash column chromatography (15 g $SiO_2$, 0 to 8% MeOH in DCM) to yield **24** (91 mg, 34%) and the homocoupling product (59 mg). $^1$H NMR (400 MHz, $CDCl_3$): $\delta$ 1.26 (t, *J* = 7.2 Hz, 3H, $CH_3$ OEt), 1.36 (s, 1H, $CH_3$ isop), 1.40 (s, 3H, $CH_3$ isop), 1.42 (s, 9H, $CH_3$ Boc), 1.58 (s, 3H, $CH_3$ isop), 1.59-1.61 (m, 2H, $CH_2$), 1.62 (s, 3H, $CH_3$ isop), 3.05 (dd, *J* = 13.8 Hz, *J* = 4.6 Hz, 1H, H-5'b), 3.08-3.19 (m, 3H, H-5"b and $CH_2$NBoc), 3.20-3.33 (m, 2H, $NCH_2$), 3.45-3.55 (m, 3H, H-5'a and $CH_2CO$), 3.69-3.76 (m, 1H, H-5"a), 3.90 (ABq, *J* = 18 Hz, 2H, $CH_2$-C≡), 4.17 (q, *J* = 7.2 Hz, 2H, $CH_2$ OEt), 4.40-4.43 (m, 1H, H-4'a), 4.46-4.51 (m, 1H, H-4'b), 4.96 (dd, *J* = 6.2 Hz, *J* = 2.6 Hz, 1H, H-3'a), 5.01-5.08 (m, 1H, NH), 5.14 (dd, *J* = 6.4 Hz, *J* = 3.6 Hz, 1H, H-3'b), 5.45 (dd, *J* = 6.2 Hz, *J* = 3.9 Hz, 1H, H-2'a), 5.48 (dd, *J* = 6.4 Hz, *J* = 1.9 Hz, 1H, H-2'b), 6.10 (d, *J* = 3.8 Hz, 1H, H-1'a), 6.14 (d, *J* = 1.9 Hz, 1H, H-1'b), 6.19 (s, 2H, $NH_2$), 6.49 (s, 2H, $NH_2$), 6.70 (s, 1H, NH), 8.03 (s, 1H, H-8b), 8.32 (s, 1H, H-2), 8.35 (s, 1H, H-2); $^{13}$C NMR (100 MHz, $CDCl_3$): $\delta$ 14.16 ($CH_3$ OEt), 25.38, 25.45, 27.16 and 27.43 ($CH_3$ isop), 28.40 (3C, $CH_3$ Boc), 31.05 ($CH_2$), 37.11 ($NCH_2$), 42.17 (C-5'a), 44.66 (***C***$H_2$-C≡), 45.89 ($CH_2$), 55.26 and 55.64 ($NCH_2CO$ and C-5'b), 60.85 ($CH_2$ OEt), 73.94 (***C***≡C-$CH_2$), 79.16 (Cq *t*Bu), 81.98 (C-3'b), 82.59 (C-2'b), 82.97 (C-2'a), 83.88 (C-3'a), 85.14 (C-4'b), 86.62 (C-4'a), 90.72 (C-1'a), 90.96 (C-1'b), 92.69 (C≡***C***-$CH_2$), 114.23 and 114.49 (Cq isop), 119.90 (C-5a), 119.98 (C-5b), 134.10 (C-8a), 140.21 (C-8b), 148.56 (C-4b), 149.11 (C-4a), 152.86 (C-2a), 153.55 (C-2b), 155.46 (C-6a), 155.66 (C-6b), 156.46 (CO Boc), 158.91 (CO urea), 170.33 (COOEt); HRMS (ESI-TOF): *m/z* calcd for $[C_{42}H_{58}N_{14}O_{11}+H]^+$ 935.4482 found 935.4483.

**5'-Deoxy-5'-[*N*-(3-(5'-deoxy-5'-(3-(3-aminopropyl)ureido)-adenosine-8-yl)prop-2-yn-1-yl)-2-(acetic acid)amino]-adenosine (26)**

To a solution of **24** (91 mg, 0.1 mmol) in water (0.5 mL) and 1,4-dioxane (0.5 mL) was added NaOH (2 N in water, 56 µL, 0.12 mmol). After 2 h at room temperature, the mixture was cooled down to 0°C before adding an ice-cold solution of TFA (50% in water, 1.0 mL). After 5 h at room temperature, volatiles were removed by lyophilization. The residue was purified by reverse phase HPLC (0–50% acetonitrile in 10 mM TEAA buffer, linear gradient over 15 min, $t_R$ = 7.8 min) to yield **26** (43 mg, 61%). $^1$H NMR (400 MHz, DMSO-$d_6$): $\delta$ 1.59-1.68 (m, 2H, $CH_2$), 2.75 (t, $J$ = 7.2 Hz, 2H, $CH_2$), 2.95-3.11 (m, 4H, $CH_2$, H-5'b and H-5"b), 3.12-3.21 (m, 2H, $NCH_2CO$), 3.22-3.31 (m, 1H, H-5'a), 3.33-3.41 (m, 1H, H-5''a), 3.88 (br, 2H, ***C***$H_2$-C≡), 3.92-4.00 (m, 2H, H-3'a and H-4'a), 4.01-4.06 (m, 1H, H-4'b), 4.20 (t, $J$ = 4.98 Hz, 1H, H-3'b), 4.63 (t, $J$ = 5.2 Hz, 1H, H-2'b), 4.97 (t, $J$ = 6.4 Hz, 1H, H-2'a), 5.89 (d, $J$ = 5.0 Hz, 1H, H-1'b), 6.16 (d, $J$ = 6.9 Hz, 1H, H-1'a), 6.20 (t, $J$ = 6.0 Hz, 1H, NHCO), 6.47 (t, $J$ = 5.6 Hz, 1H, NH-5'), 7.25 (s, 2H, $NH_2$), 7.48 (s, 2H, $NH_2$), 8.17 (s, 1H, H-2b), 8.21 (s, 1H, H-2a), 8.41 (s, 1H, H-8b); $^{13}$C NMR (100 MHz, DMSO-$d_6$): $\delta$ 29.00 ($CH_2$), 36.50 ($NCH_2$), 36.98 ($NCH_2$), 42.64 (C-5'a), 44.62 (***C***$H_2$-C≡), 56.20 (C-5'b), 59.46 ($NCH_2CO$), 71.74 (C-3'a), 72.03 (C-2'a), 72.33 (C-3'b), 73.52 (C-2'b), 74.37 (***C***≡C-$CH_2$), 83.19 (C-4'b), 85.21 (C-4'a), 87.92 (C-1'b), 88.76 (C-1'a), 94.19 (C≡***C***-$CH_2$), 119.51 (2C, C-5a and C-5b), 134.07 (C-8a), 140.15 (C-8b), 149.32 (C-4a), 149.93 (C-4b), 153.14 (C-2b), 154.04 (C-2a), 156.39 and 156.49 (C-6a and C-6b), 159.20 (CO urea), 175.11 (CO); HRMS (ESI-TOF): *m/z* calcd for $[C_{29}H_{38}N_{14}O_9+H]^+$ 727.3019, found 727.3022.

**Macrocycle MC6**

A solution of **26** (20.0 mg, 0.027 mmol) and DIEA (41 µL, 0.08 mmol) in DMF (2.8 mL) was added dropwise (over 4 h) to a solution of PyBOP (31 mg, 0.06 mmol) in DMF (300 µL). After stirring for 18 h at room temperature, PyBOP (31 mg) and DIEA (41 µL) were added for reaction completion. After 16 h at room temperature, DMF was removed under reduced pressure and the residue was purified by reverse phase HPLC (5–15% acetonitrile in 10 mM TEAA buffer, linear gradient over 15 min, $t_R$ = 13.1 min) to yield **MC6** (5.0 mg, 25%). $^1$H NMR (400 MHz, DMSO-$d_6$): $\delta$ 1.42-1.56 (m, 2H, $CH_2$), 2.91-3.29 (m, 9H, H-5'b, H-5"b, H-5'a, $NHCH_2$, $CH_2NH$, $NCH_2CO$), 3.48-3.57 (m, 1H, H-5"a), 3.80 (ABq, $J$ = 17.8 Hz, 2H, $CH_2$-C≡), 3.83-3.89 (m, 1H, H-4'a), 4.07-4.14 (m, 2H, H-3'a and H-4'b), 4.20-4.25 (m, 1H, H-3'b), 4.65 (q, $J$ = 5.3 Hz, 1H, H-2'b), 4.90 (q, $J$ = 5.6 Hz, 1H, H-2'a), 5.17 (d, $J$ = 5.6 Hz, 1H, OH-3'a), 5.27 (d, $J$ = 5.3 Hz, 1H, OH-3'b), 5.40 (d, $J$ = 5.7 Hz, 1H, OH-2'a), 5.48 (d, $J$ = 5.7 Hz, 1H, OH-2'b) 5.85-5.90 (m, 2H, 2 NH urea), 5.91 (d, $J$ = 5.2 Hz, 1H, H-1'b), 6.00 (d, $J$ = 5.2 Hz, 1H, H-1'a), 7.24 (s, 2H, $NH_2$), 7.53 (s, 2H, $NH_2$), 7.59 (br t, 1H, NHCO), 8.16 (s, 1H, H-2b), 8.19 (s, 1H, H-2a), 8.36 (s, 1H, H-8b); $^{13}$C NMR (100 MHz, DMSO-$d_6$): $\delta$ 29.66 ($CH_2$), 37.92 ($CH_2$), 39.20 ($CH_2$), 42.05 (C-5'a), 44.68 (***C***$H_2$-C≡), 56.91 (C-5'b), 57.91 ($NCH_2CO$), 71.00 (C-3'a), 71.96 and 72.19 (C-2'a and C-3'b), 73.22 (C-2'b), 75.42 (***C***≡C-$CH_2$), 82.91 and 83.13 (C-4'b and C-4'a), 88.15 (C-1'b), 88.43 (C-1'a), 93.01 (C≡***C***-$CH_2$), 118.78 (C-5a), 119.58 (C-5b), 132.57 (C-8a), 140.17 (C-8b), 149.86 (C-4b), 149.93 (C-4a), 153.17 (C-2b), 154.37 (C-2a), 156.28 and 156.51 (C-6a and C-6b), 158.86 (CO urea), 169.51 (CO); HRMS (ESI-TOF): *m/z* calcd for $[C_{29}H_{36}N_{14}O_8+H]^+$ 709.2913 found 709.2905.

*4.4. In vitro enzymatic activity inhibition assays*

NADK1 of *L. monocytogenes* (EC 2.7.1.23) with a 6-His tag at the C-terminus was expressed and purified as described previously [19]. The enzymatic reaction was followed at 30°C in a CLARIOstar plate reader (BMG LABTECH) by measuring the absorbance at 340 nm ($OD_{340}$) using an enzymatic coupled system involving glucose-6-phosphate dehydrogenase (G6PDH). The reaction mixture was made in a half area 96-well microplate (Greiner Bio-One Clear UV-Star). Buffer used were 50 mM Bis-Tris pH 7.0, 2 mM NaCitrate Tribasic Dihydrate, 1 mM $MgCl_2$. Reaction mixtures contained 25 nM *Lm*NADK1, 0.1-2 mM NAD (12 different concentrations), 4 mM MgATP, 5 mM glucose-6-phosphate, 1 U/mL G6PDH and 4–8 different concentrations of inhibitors in the range of the $K_i$ values. Buffer, NAD and inhibitor solutions (total volume 25 µL, concentration 4×) were dispensed into the microplate using an OT-2 lab robot (Opentrons). 25 µL of a mixture containing G6PDH, MgATP and glucose-6-phosphate at a 4× concentration were dispensed using a manual repeating pipette. Finally, the reaction was started at time 0 by adding and mixing 50 µL of *Lm*NADK1 at a 2× concentration using a multichannel pipette. $OD_{340}$ were measured every 32 s during 32 min. The values of the inhibition constants were determined by global fittings of the steady state rate constants, $k_{ss}$, at different concentrations of NAD and inhibitor, with a competitive inhibition equation using GraFit software (version 7.0.3, Erithacus Software Ltd). The inhibition assays were carried out in independent triplicates.

*4.5. Antibacterial activity*

Overnight cultures of either *S. aureus* Xen36 (Caliper Life Science) or *L. monocytogenes* EGDe (BUG1600) in BHI at 37°C were diluted 1:100 into BHI broth. For *S. aureus* growth inhibition assay, BHI broth was supplemented with 25% PBS/10% DMSO (negative control), 10 µg/mL levofloxacin (positive control), NKI1 [15] or cyclic compounds (this study) in 25% PBS/10 % DMSO. For *L. monocytogenes* growth inhibition assay, BHI broth was supplemented with 25% PBS/1% DMSO (negative control), 10 µg/mL levofloxacin (positive control), NKI1 or cyclic compounds in in 25% PBS/1% DMSO. Growth inhibition was also determined for each cyclic compounds with polymyxin B at 20, 40, 60 and 80 µg/mL in BHI supplemented with 25% PBS/10% DMSO (for *S. aureus*) or 25% PBS/1% DMSO (for *L. monocytogenes)*. Bacterial suspensions were incubated in 96-well plates, with shaking at 200 rpm at 37°C. Growth was monitored with a microplate reader (Glomax Discover, Promega).

*4.6. Comparative modeling*

The structure of the NADK from *S. aureus* was modeled based on various conformation of *Lm*NADK1 using the webserver @TOME-2 [43]. These models were superposed to the new complexes of *Lm*NADK1 solved

in this study to evaluate the specific protein-ligand interactions due to some residue substitutions observed in the active site (especially T133 in *Sa*NADK instead of P132 in *Lm*NADK1).

**Acknowledgments**

This work was funded by the Agence Nationale de la Recherche (NADKiller, ANR-17-CE18-0011-02) and supported by Institut Pasteur, the Centre National de la Recherche Scientifique (CNRS), Institut National de la Santé et de la Recherche Médicale (INSERM) and University of Montpellier. C.L. and D.A.C. acknowledge ANR for financial support. This work was also supported by the French Infrastructure for Integrated Structural Biology (FRISBI, ANR-10-INSB-05-01). We acknowledge the experimental assistance from the staff of the European Synchrotron Radiation Facility (ESRF, Grenoble, France, beamlines ID23-2, ID30-A1, ID30-A3) and the synchrotron ALBA (Barcelona, Spain, beamline BL13-XALOC) during data collection. The authors would like to thank Frédéric Bonhomme (CNRS, UMR3523, Institut Pasteur) for assisting with HRMS analysis.

**Appendix A Supporting information/ Supplementary data**

Supplementary data related to this article can be found at http://

**Accession Codes**

The crystal structures of *Lm*NADK1 bound to the macrocycles **MC1-6** are deposited under accession codes PDB: 8B47, 7ZZH, 7ZZJ, 7ZZF, 7ZZG and 7ZZE, respectively. The complexes of *Lm*NADK1 with the acyclic precursors are available in the PDB under the accession codes: 7ZZ7, 7ZZ9, 7ZZA, 7ZZB, 7ZZC, 7ZZD and 8A9V.

**References**

1. Tacconelli, E.; Sifakis, F.; Harbarth, S.; Schrijver, R.; van Mourik, M.; Voss, A.; Sharland, M.; Rajendran, N.B.; Rodríguez-Baño, J. Surveillance for control of antimicrobial resistance. *Lancet Infect Dis* **2018**, *18*, e99-e106, doi:10.1016/s1473-3099(17)30485-1.
2. McGuinness, E.T.; Butler, J.R. NAD+ kinase—A review. *Int J Biochem* **1985**, *17*, 1-11, doi:10.1016/0020-711X(85)90079-5.
3. Magni, G.; Orsomando, G.; Raffaelli, N. Structural and functional properties of NAD kinase, a key enzyme in NADP biosynthesis. *Mini Rev Med Chem* **2006**, *6*, 739-746, doi:10.2174/138955706777698688.
4. Kawai, S.; Murata, K. Structure and Function of NAD Kinase and NADP Phosphatase: Key Enzymes That Regulate the Intracellular Balance of NAD(H) and NADP(H). *Biosci Biotechnol Biochem* **2008**, *72*, 919-930, doi:10.1271/bbb.70738.
5. Bi, J.; Wang, H.; Xie, J. Comparative genomics of NAD(P) biosynthesis and novel antibiotic drug targets. *J Cell Physiol* **2011**, *226*, 331-340, doi:10.1002/jcp.22419.
6. Murata, K. Polyphosphate-dependent nicotinamide adenine dinucleotide (NAD) kinase: A novel missing link in human mitochondria. *Proc Jpn Acad B: Phys Biol Sci* **2021**, *97*, 479-498, doi:10.2183/pjab.97.0{Gerdes, 2002 #14}24.

7. Kornberg, A.; Pricer, W.E. On the structure of triphosphopyridine nucleotide. *J Biol Chem* **1950**, *186*, 557-567, doi:10.1016/S0021-9258(18)56249-9.
8. Kawai, S.; Mori, S.; Mukai, T.; Suzuki, S.; Yamada, T.; Hashimoto, W.; Murata, K. Inorganic Polyphosphate/ATP-NAD kinase of Micrococcus flavus and Mycobacterium tuberculosis H37Rv. *Biochem Biophys Res Commun* **2000**, *276*, 57-63, doi:10.1006/bbrc.2000.3433.
9. Lerner, F.; Niere, M.; Ludwig, A.; Ziegler, M. Structural and Functional Characterization of Human NAD Kinase. *Biochem Biophys Res Commun* **2001**, *288*, 69-74, doi:10.1006/bbrc.2001.5735.
10. Labesse, G.; Douguet, D.; Assairi, L.; Gilles, A.-M. Diacylglyceride kinases, sphingosine kinases and NAD kinases: distant relatives of 6-phosphofructokinases. *Trends Biochem Sci* **2002**, *27*, 273-275, doi:10.1016/S0968-0004(02)02093-5.
11. Mary, C.; Soflaee, M.H.; Kesavan, R.; Gelin, M.; Brown, H.; Zacharias, G.; Mathews, T.P.; Lemoff, A.; Lionne, C.; Labesse, G., et al. Crystal structure of human NADK2 reveals a dimeric organization and active site occlusion by lysine acetylation. *Mol Cell* **2022**, *82*, 3299-+, doi:10.1016/j.molcel.2022.06.026.
12. Kobayashi, K.; Ehrlich, S.D.; Albertini, A.; Amati, G.; Andersen, K.K.; Arnaud, M.; Asai, K.; Ashikaga, S.; Aymerich, S.; Bessieres, P., et al. Essential Bacillus subtilis genes. *Proc. Natl. Acad. Sci. U.S.A.* **2003**, *100*, 4678, doi:10.1073/pnas.0730515100.
13. Sassetti, C.M.; Boyd, D.H.; Rubin, E.J. Genes required for mycobacterial growth defined by high density mutagenesis. *Mol Microbiol* **2003**, *48*, 77-84, doi:10.1046/j.1365-2958.2003.03425.x.
14. Chaudhuri, R.R.; Allen, A.G.; Owen, P.J.; Shalom, G.; Stone, K.; Harrison, M.; Burgis, T.A.; Lockyer, M.; Garcia-Lara, J.; Foster, S.J., et al. Comprehensive identification of essential Staphylococcus aureus genes using Transposon-Mediated Differential Hybridisation (TMDH). *BMC Genom.* **2009**, *10*, 291, doi:10.1186/1471-2164-10-291.
15. Gelin, M.; Paoletti, J.; Nahori, M.A.; Huteau, V.; Leseigneur, C.; Jouvion, G.; Dugue, L.; Clement, D.; Pons, J.L.; Assairi, L., et al. From Substrate to Fragments to Inhibitor Active In Vivo against Staphylococcus aureus. *ACS Infect. Dis.* **2020**, *6*, 422-435, doi:10.1021/acsinfecdis.9b00368.
16. Gerdes, S.Y.; Scholle, M.D.; D'Souza, M.; Bernal, A.; Baev, M.V.; Farrell, M.; Kurnasov, O.V.; Daugherty, M.D.; Mseeh, F.; Polanuyer, B.M., et al. From Genetic Footprinting to Antimicrobial Drug Targets: Examples in Cofactor Biosynthetic Pathways. *J Bacteriol* **2002**, *184*, 4555-4572, doi:10.1128/jb.184.16.4555-4572.2002.
17. Magni, G.; Di Stefano, M.; Orsomando, G.; Raffaelli, N.; Ruggieri, S. NAD(P) Biosynthesis Enzymes as Potential Targets for Selective Drug Design. *Curr Med Chem* **2009**, *16*, 1372-1390, doi:10.2174/092986709787846505.
18. Depaix, A.; Kowalska, J. NAD Analogs in Aid of Chemical Biology and Medicinal Chemistry. *Molecules* **2019**, *24*, 4187, doi:doi.org/10.3390/molecules24224187.
19. Poncet-Montange, G.; Assairi, L.; Arold, S.; Pochet, S.; Labesse, G. NAD kinases use substrate-assisted catalysis for specific recognition of NAD. *J Biol Chem* **2007**, *282*, 33925-33934, doi:10.1074/jbc.M701394200.
20. Gelin, M.; Poncet-Montange, G.; Assairi, L.; Morellato, L.; Huteau, V.; Dugué, L.; Dussurget, O.; Pochet, S.; Labesse, G. Screening and In Situ Synthesis Using Crystals of a NAD Kinase Lead to a Potent Antistaphylococcal Compound. *Structure* **2012**, *20*, 1107-1117, doi:0.1016/j.str.2012.03.024.
21. Paoletti, J.; Assairi, L.; Gelin, M.; Huteau, V.; Nahori, M.-A.; Dussurget, O.; Labesse, G.; Pochet, S. 8-Thioalkyl-adenosine derivatives inhibit Listeria monocytogenes NAD kinase through a novel binding mode. *Eur J Med Chem* **2016**, *124*, 1041-1056, doi:10.1016/j.ejmech.2016.10.033.
22. Clement, D.A.; Leseigneur, C.; Gelin, M.; Coelho, D.; Huteau, V.; Lionne, C.; Labesse, G.; Dussurget, O.; Pochet, S. New Chemical Probe Targeting Bacterial NAD Kinase. *Molecules* **2020**, *25*, E4893, doi:10.3390/molecules25214893.
23. Kho, R.; Baker, B.L.; Newman, J.V.; Jack, R.M.; Sem, D.S.; Villar, H.O.; Hansen, M.R. A path from primary protein sequence to ligand recognition. *Proteins* **2003**, *50*, 589-599, doi:10.1002/prot.10316.

24. Fujii, M.; Kitagawa, Y.; Iida, S.; Kato, K.; Ono, M. Novel concept of enzyme selective nicotinamide adenine dinucleotide (NAD)-modified inhibitors based on enzyme taxonomy from the diphosphate conformation of NAD. *Bioorg Med Chem Lett* **2015**, *25*, 5133-5136, doi:10.1016/j.bmcl.2015.10.005.
25. Marsault, E.; Peterson, M.L. Macrocycles Are Great Cycles: Applications, Opportunities, and Challenges of Synthetic Macrocycles in Drug Discovery. *J Med Chem* **2011**, *54*, 1961-2004, doi:10.1021/jm1012374.
26. Martí-Centelles, V.; Pandey, M.D.; Burguete, M.I.; Luis, S.V. Macrocyclization Reactions: The Importance of Conformational, Configurational, and Template-Induced Preorganization. *Chem Rev* **2015**, *115*, 8736-8834, doi:10.1021/acs.chemrev.5b00056.
27. Jwad, R.; Weissberger, D.; Hunter, L. Strategies for Fine-Tuning the Conformations of Cyclic Peptides. *Chem Rev* **2020**, *120*, 9743-9789, doi:10.1021/acs.chemrev.0c00013.
28. Huang, M.L.; Shin, S.B.Y.; Benson, M.A.; Torres, V.J.; Kirshenbaum, K. A Comparison of Linear and Cyclic Peptoid Oligomers as Potent Antimicrobial Agents. *ChemMedChem* **2012**, *7*, 114-122, doi:10.1002/cmdc.201100358.
29. Amrhein, J.A.; Knapp, S.; Hanke, T. Synthetic Opportunities and Challenges for Macrocyclic Kinase Inhibitors. *J Med Chem* **2021**, *64*, 7991-8009, doi:10.1021/acs.jmedchem.1c00217.
30. Bechtler, C.; Lamers, C. Macrocyclization strategies for cyclic peptides and peptidomimetics. *RSC Med Chem* **2021**, *12*, 1325-1351, doi:10.1039/d1md00083g.
31. Kurz, C.G.; Preuss, F.; Tjaden, A.; Cusack, M.; Amrhein, J.A.; Chatterjee, D.; Mathea, S.; Berger, L.M.; Berger, B.-T.; Krämer, A., et al. Illuminating the Dark: Highly Selective Inhibition of Serine/Threonine Kinase 17A with Pyrazolo[1,5-a]pyrimidine-Based Macrocycles. *J Med Chem* **2022**, *65*, 7799-7817, doi:10.1021/acs.jmedchem.2c00173.
32. Liu, J.; Leonard, P.; Müller, S.L.; Daniliuc, C.; Seela, F. Nucleoside macrocycles formed by intramolecular click reaction: efficient cyclization of pyrimidine nucleosides decorated with 5'-azido residues and 5-octadiynyl side chains. *Beilstein J Org Chem* **2018**, *14*, 2404-2410, doi:10.3762/bjoc.14.217.
33. Lietard, J.; Meyer, A.; Vasseur, J.J.; Morvan, F. New strategies for cyclization and bicyclization of oligonucleotides by click chemistry assisted by microwaves. *J Org Chem* **2008**, *73*, 191-200, doi:10.1021/jo702177c.
34. Sangouard, G.; Zorzi, A.; Wu, Y.; Ehret, E.; Schüttel, M.; Kale, S.; Díaz-Perlas, C.; Vesin, J.; Bortoli Chapalay, J.; Turcatti, G., et al. Picomole-Scale Synthesis and Screening of Macrocyclic Compound Libraries by Acoustic Liquid Transfer. *Angew Chem Int Ed* **2021**, *60*, 21702-21707, doi:10.1002/anie.202107815.
35. Kan, T.; Fukuyama, T. Ns strategies: a highly versatile synthetic method for amines. *Chem Comm* **2004**, 10.1039/B311203A, 353-359, doi:10.1039/B311203A.
36. Benedetto Tiz, D.; Kikelj, D.; Zidar, N. Overcoming problems of poor drug penetration into bacteria: challenges and strategies for medicinal chemists. *Expert Opinion on Drug Discovery* **2018**, *13*, 497-507, doi:10.1080/17460441.2018.1455660.
37. Prajapati, J.D.; Kleinekathöfer, U.; Winterhalter, M. How to Enter a Bacterium: Bacterial Porins and the Permeation of Antibiotics. *Chemical Reviews* **2021**, *121*, 5158-5192, doi:10.1021/acs.chemrev.0c01213.
38. Zeiders, S.M.; Chmielewski, J. Antibiotic–cell-penetrating peptide conjugates targeting challenging drug-resistant and intracellular pathogenic bacteria. *Chemical Biology & Drug Design* **2021**, *98*, 762-778, doi:https://doi.org/10.1111/cbdd.13930.
39. Mallinson, J.; Collins, I. Macrocycles in new drug discovery. *Future Medicinal Chemistry* **2012**, *4*, 1409-1438, doi:10.4155/fmc.12.93.
40. Emsley, P.; Lohkamp, B.; Scott, W.G.; Cowtan, K. Features and development of Coot. *Acta Crystallogr D* **2010**, *66*, 486-501, doi:10.1107/S0907444910007493.
41. Korb, O.; Stützle, T.; Exner, T.E. PLANTS: Application of Ant Colony Optimization to Structure-Based Drug Design. In Proceedings of Ant Colony Optimization and Swarm Intelligence, Berlin, Heidelberg, 2006//; pp. 247-258.

42. Adams, P.D.; Afonine, P.V.; Bunkóczi, G.; Chen, V.B.; Davis, I.W.; Echols, N.; Headd, J.J.; Hung, L.W.; Kapral, G.J.; Grosse-Kunstleve, R.W., et al. PHENIX: a comprehensive Python-based system for macromolecular structure solution. *Acta Crystallogr D Biol Crystallogr* **2010**, *66*, 213-221, doi:10.1107/s0907444909052925.

43. Pons, J.L.; Labesse, G. @TOME-2: a new pipeline for comparative modeling of protein-ligand complexes. *Nucleic. Acids Res.* **2009,** *37*, W485-491.